Journal of Ceramic Processing Research. Vol. 26, No. 5, pp. 717~725 (2025)
(Received 16 May 2025, Received in revised form 17 July 2025, Accepted 24 July 2025)
https://doi.org/10.36410/jcpr.2025.26.5.717

J O U R N A L O F
Ceramic Processing Research

Physicochemical properties of hydroxyapatite from *Polymesoda erosa* shells and antibacterial potential of HA-ZnO composites

Endang Haryati[a,b], Jumiarti Andi Lolo[a,c], Ahmad Kusumaatmaja[a] and Yusril Yusuf[a,*]
[a]*Department of Physics, Faculty of Mathematics and Natural Science, Universitas Gadjah Mada, Yogyakarta 55281, Indonesia*
[b]*Department of Physics, Faculty of Mathematics and Natural Science, Universitas Cenderawasih, Jayapura 99351, Indonesia*
[c]*Department of Physics Education, Faculty of Teacher Training and Education, Universitas Kristen Indonesia Toraja, Tana Toraja, 91811, Indonesia*

This study investigated the physicochemical properties of hydroxyapatite (HA) synthesized from *Polymesoda erosa* shells and the antibacterial potential of HA combined with zinc oxide (ZnO). *Polymesoda erosa* shells were calcined to produce calcium oxide (CaO), which was subsequently used to synthesize HA via precipitation. Hydroxyapatite (HA) was synthesized and subsequently characterized by X-ray diffraction (XRD), Fourier-transform infrared spectroscopy (FTIR), and scanning electron microscopy (SEM). The results indicated high crystallinity and a calcium-to-phosphorus (Ca/P) molar ratio ranging from 1.52 to 1.69, closely resembling the composition of natural bone. At higher sintering temperatures, partial transformation to β-tricalcium phosphate (β-TCP) was observed, enhancing bioactivity. The antibacterial properties were assessed using the disk diffusion technique. While pure hydroxyapatite (HA) exhibited no observable inhibition zones, the addition of 1.5% zinc oxide (ZnO) significantly enhanced antibacterial performance, as evidenced by inhibition zones measuring 0.96 mm against *Staphylococcus aureus* and 0.62 mm against *Escherichia coli*. These results suggest that ZnO incorporation effectively imparts antibacterial activity to the HA matrix. The results highlighted the potential of *Polymesoda erosa*-derived HA-ZnO composites as sustainable biomaterials for regenerative bone applications. Their enhanced bioactivity and antibacterial properties make them promising candidates for advancing suggest their promise in advancing bone tissue engineering and addressing infection-related challenges.

Keywords: *Polymesoda erosa*, Hydroxyapatite, Zinc oxide, Composite, Antibacterial.

Introduction

Hydroxyapatite (HA), chemically denoted as $Ca_{10}(PO_4)_6(OH)_2$, is the primary inorganic component of human bones and teeth, providing essential structural support and biological functionality [1–3]. Its excellent biocompatibility, osteoconductivity, and similarity to the mineral phase of bone make HA indispensable in biomedical applications. These include its use in bone grafts, dental implants, and scaffolds for tissue engineering [2,4]. HA is particularly valued for promoting osseointegration, enabling implants to integrate securely with surrounding bone tissue, while fostering osteoblast proliferation, which is critical for bone repair and regeneration [5,6]. Additionally, HA's versatility extends to oncology, where its nanoparticles have demonstrated promising results in inhibiting tumour cell proliferation, thereby expanding its potential applications [7]. The sustainability of HA production has emerged as a priority due to the high costs and environmental impact of synthetic methods. Natural sources, such as marine organisms, provide an eco-friendly alternative, offering HA with a chemical composition resembling human bone. Marine-derived HA often contains trace elements like magnesium and strontium, which enhance bioactivity and osteoconductivity [8,9]. Furthermore, utilizing marine by-products such as fish bones, cuttlefish, and mollusc shells reduces environmental waste while generating high-value materials for biomedical applications [10,11]. Despite the progress in exploring traditional marine sources, significant potential remains for exploring novel, underutilized materials for HA production.

Synthetic HA, while effective, faces limitations such as high production costs, significant environmental impact, and limited resemblance to natural bone structures [3,4]. These challenges underscore the need for innovative approaches to HA synthesis, particularly from renewable resources. Among these, *Polymesoda erosa* shells present a promising yet underexplored option. Abundant and sustainable, these shells offer a cost-effective source of HA [2]. However, limited research has been conducted to characterize the HA derived from *Polymesoda erosa* shells comprehensively.

*Corresponding author:
Tel : +62-0274-6492383
Fax: +62-0274-6492383
E-mail: yusril@ugm.ac.id

Key properties such as crystallinity, porosity, and bioactivity remain insufficiently explored, which presents opportunities for further research into their potential as advanced biomaterials. While HA is widely used in biomedical applications, its susceptibility to bacterial infections, particularly in orthopedic and dental implants, poses significant challenges. Researchers have developed HA composites incorporating antimicrobial agents such as zinc oxide (ZnO) to address this issue. ZnO is well-known for broad-spectrum antibacterial properties and ability to enhance HA's functionality in combating infections [12,13].

The antimicrobial performancecc of ZnO nanoparticles is primarily attributed to the generation of Reactive Oxygen Species (ROS), the release of Zn^{2+} ions, and the disruption of bacterial cell membrane integrity, thereby effectively inhibiting the growth of both Gram-positive and Gram-negative bacterial strains [14,15]. Studies have demonstrated the efficacy of HA-ZnO composites in reducing bacterial growth and biofilm formation, making them suitable for applications requiring infection prevention ([13,16]. For instance, incorporating ZnO nanoparticles into dental composites significantly enhances their antibacterial performance without compromising mechanical properties [16]. Similarly, HA-ZnO composites facilitate bone regeneration and infection resistance, demonstrating their dual functionality [13]. In addition to antimicrobial properties, ZnO nanoparticles improve the physicochemical characteristics of HA. Their incorporation enhances HA's crystallinity, porosity, and mechanical strength, making it suitable for load-bearing applications [12,13]. However, while synthetic HA-ZnO composites have shown great promise, limited research has focused on integrating ZnO with naturally derived HA from marine sources, particularly P. erosa shells. This represents a critical gap, as leveraging renewable sources in combination with ZnO could yield advanced and sustainable biomaterials.

Polymesoda erosa shells offer significant potential as a renewable source of Hydroxyapatite. Nasution et al. (2021) demonstrated that HA derived from these shells closely resembles natural bone, making it a promising candidate for biomedical applications. However, detailed characterization of crystallinity, morphology, and porosity properties is necessary to assess their suitability for advanced uses. Furthermore, while ZnO's antibacterial efficacy is well-documented, its integration with naturally derived HA, especially from marine sources, remains insufficiently explored [12,13]. Optimizing the concentration and distribution of ZnO within HA matrices is essential for balancing antibacterial efficacy with biocompatibility [14,17]. This research aims to bridge existing knowledge gaps by synthesizing hydroxyapatite (HA) derived from *Polymesoda erosa* shells and systematically characterizing its physicochemical properties through advanced analytical methods, including X-ray diffraction (XRD), scanning electron microscopy (SEM), and Fourier-transform infrared spectroscopy (FTIR). Furthermore, the antibacterial performance of HA-ZnO composites was assessed against representative bacterial strains, namely *Staphylococcus aureus* and *Escherichia coli*. By employing *Polymesoda erosa* shells as a renewable biogenic precursor, this study seeks to develop multifunctional biomaterials with improved physicochemical and antimicrobial characteristics, thereby promoting sustainable approaches in biomedical material design.

Materials and Methods

Materials

The primary materials used in this study included mangrove shells (*Polymesoda erosa*), collected from Youtefa Bay, Jayapura City, Papua, Indonesia. Additional materials were included diammonium hydrogen phosphate ($(NH_4)_2HPO_4$) and zinc oxide (ZnO), both obtained from Merck, Germany.

Method

The production of calcium oxide (CaO) from *Polymesoda erosa* shells

The mangrove shell waste collected from Youtefa Bay was initially cleaned of macro and micro-impurities using water, followed by boiling and sun-drying for 24 hours. The dried shells were soaked in acetone for 24 hours to eliminate residual contaminants and then rinsed thoroughly with water. A final wash with distilled water (deionized water) ensured the removal of all dirt and moss adhering to the shells. After cleaning, the shells were oven-dried at 100 °C for 6 hours. The dried shells were chopped into smaller pieces and ground using a ball mill to achieve a fine powder. A portion of this powder was sieved through a 200-mesh sieve to ensure uniform particle size. The fine *Polymesoda erosa* shell powder was calcined at temperatures of 800 °C, 900 °C, and 1000 °C to convert calcium carbonate ($CaCO_3$) into calcium oxide (CaO). The calcination process follows the chemical reaction shown in Equation (1):

$$CaCO_3 \rightarrow CaO + CO_2 \quad (1)$$

Synthesis of Hydroxyapatite

Hydroxyapatite (HA) was synthesized via a wet chemical precipitation method. CaO was obtained by calcining *Polymesoda erosa* shells and subsequently dissolved in distilled water to prepare a 1 M calcium hydroxide [$Ca(OH)_2$] solution. The solution was stirred at 450 rpm for 60 minutes at room temperature. Separately, a 0.6 M solution of $(NH_4)_2HPO_4$ was prepared. This phosphate solution was gradually added dropwise to the calcium hydroxide solution under constant stirring (450 rpm), with the temperature maintained at 60 °C for 60 minutes. During titration, the pH was continuously monitored and adjusted to remain above 9 to ensure

favorable conditions for HA precipitation. After completion of the reaction, the suspension was aged at room temperature for 24 hours to stabilize the precipitate. The solid phase was then separated by centrifugation at 3500 rpm for 5 minutes, followed by drying at 100 °C for 5 hours. Finally, the dried HA powder was calcined at 700 °C, 800 °C, 900 °C, and 1000 °C for 3.5 hours to improve crystallinity and phase purity.

Synthesis of Zinc Oxide (ZnO)-Doped Hydroxyapatite (HA)

To prepare HA doped with zinc oxide (ZnO), the HA synthesized at a sintering temperature of 700 °C was selected. ZnO powder was added to the HA powder at concentrations of 1.5% (w/w). The powders were thoroughly mixed using a mortar and pestle a mechanical mixer, to ensure homogeneity. The powder mixture was gradually mixed with deionized water until a uniform paste was obtained. The resulting paste was then compacted into the desired shape using stainless steel molds. The molded paste was sintered at 700 °C for 3 hours, consolidating the HA-ZnO composite and enhancing its structural properties. The resulting ZnO-doped HA composites were subsequently characterized to assess their antibacterial properties.

Physicochemical Characterization

Scanning Electron Microscopy-Energy Dispersive X-Ray Spectroscopy (SEM-EDX)

Scanning Electron Microscopy (SEM) combined with Energy Dispersive X-ray Spectroscopy (EDX) was employed to investigate the surface morphology and minerals composition of *Polymesoda erosa* shell powder, CaO, and the synthesized HA. SEM imaging was performed using a high-resolution electron microscope to observe the materials' particle size, shape, and distribution. EDX analysis was performed to determine the minerals composition and assess the purity of the samples by detecting essential elements such as calcium (Ca), phosphorus (P), oxygen (O), along with other trace constituents. These analyses were essential for evaluating the material transformation from raw shell powder to CaO and HA, providing insights into their structural integrity and suitability for biomedical applications.

X-Ray Diffraction (XRD)

X-ray Diffraction (XRD) analysis was performed to investigate the crystalline structure, phase composition, and purity of *Polymesoda erosa* shell powder, CaO, and HA. The analysis was carried out using an X-ray diffractometer equipped with Cu-Kα radiation (λ = 1.5406 Å) at 40 kV and 30 mA. Diffraction patterns were recorded within a 2θ range of 20°–80° with a step size of 0.02° and a scan speed of 2° per minute. The resulting XRD spectra were compared with reference data from the International Centre for Diffraction Data (ICDD) database to identify the crystalline phases. This analysis was essential for verifying the phase transformation and confirming the structural integrity of the synthesized materials.

Fourier Transform Infrared (FTIR)

Fourier Transform Infrared Spectroscopy (FTIR) analysis was conducted to identify the functional groups and chemical bonds in *Polymesoda erosa* shell powder, CaO, and HA. The analysis was performed using an FTIR spectrometer over the wavelength range of 4000–400 cm^{-1} with a resolution of 4 cm^{-1}. The spectra were obtained using the KBr pellet method to improve signal clarity. Characteristic absorption bands corresponding to carbonate (CO_3^{2-}), phosphate (PO_4^{3-}), hydroxyl (OH^-), and calcium-oxygen (Ca–O) bonds were identified, which helped confirm the presence and transformation of chemical compounds. This analysis was critical for verifying phase formation, detecting residual organic materials, and evaluating the chemical stability of the synthesized materials.

Antibacterial Properties

The antibacterial performance of the HA-ZnO composites was assessed using the disk diffusion method. *Staphylococcus aureus* (*S. Aureus*) and *Escherichia coli* (*E. coli*) were cultured to a concentration equivalent to 1×10^8 CFU/mL. A uniform bacterial lawn was created by spreading the bacterial suspension onto Mueller-Hinton Agar plates. Sterile filter paper discs were immersed in the HA-ZnO composite solution containing 1.5% ZnO and placed on the surface of the agar plates. Following incubation at 37 °C for 24 hours, the inhibition zones surrounding the discs were measured. The diameter of the inhibition zones, recorded in millimeters, was used to evaluate the antibacterial efficacy of the composites.

Result and Discussion

Characterization of *Polymesoda erosa* shells and Calcium oxide (CaO)

The mineral composition analysis of *Polymesoda erosa* shell powder revealed a high $CaCO_3$ content, consistent with prior studies showing bivalve shells as rich in $CaCO_3$, often exceeding 95% by weight [18, 19]. As shown in Table 1, the elemental composition of the

Table 1. Mineral composition of *Polymesoda erosa* shell powder.

Element	Mass (%)			
	Raw material	calcined at 800 °C	calcined at 900 °C	calcined at 1000 °C
C	13.04	3.89	3.80	2.92
O	50.68	52.01	39.41	48.76
Na	0.43	0.40	-	-
Ca	35.95	43.70	56.79	48.31

shell powder changed significantly after calcination, with calcium (Ca) content increasing notably, peaking at 56.79% at 900 °C. This rise reflected the thermal decomposition of $CaCO_3$ into CaO. Concurrently, carbon (C) content decreased from 13.04% in the uncalcined shell to 2.92% after calcination at 1000 °C, confirming the release of carbon dioxide (CO_2) during the process. Oxygen (O) content also varied, and sodium (Na) impurities were eliminated at higher temperatures, highlighting calcination's role as an effective purification method [20–23]. These findings align with other studies emphasizing *Polymesoda erosa* shells' potential for producing high-purity CaO, which offer a sustainable, cost-effective alternative to traditional limestone-derived CaO and supports circular economy initiatives [19,20].

The phase transformation during calcination was further confirmed through XRD analysis (Fig. 1). Uncalcined samples exhibited peaks associated with aragonite and calcite, polymorphs of $CaCO_3$, indicating the crystalline nature of the shells [24,25]. These peaks diminished after calcination, were replaced with sharp peaks of CaO at 900 °C and 1000 °C, demonstrating the successful decomposition of $CaCO_3$ to CaO [26,27]. Compared to other biogenic $CaCO_3$ sources, *Polymesoda erosa* shells achieved complete conversion at 900 °C and 1000 °C, outperforming sources that retain residual carbonate phases [28,29]. FTIR analysis (Fig. 2) supported these findings by identifying molecular vibrations characteristic of carbonate and oxide groups. In uncalcined samples, bands at ~875 cm^{-1} and 1426 cm^{-1} corresponded to carbonate ions (CO_3^{2-}), while a broad O–H stretching band near 3300 cm^{-1} indicated organic and hydroxyl group presence. Post-calcination, these carbonate bands were replaced by bands near 500–600 cm^{-1}, indicative of CaO formation. This spectral shift confirmed the successful thermal decomposition of $CaCO_3$ into CaO, which occurred completely at calcination temperatures of 900 and 1000 °C, and the retention of reactive hydroxyl groups, essential for catalysis and bioceramic applications [20,28,30].

The study highlights *Polymesoda erosa* shells as a sustainable, cost-effective precursor for high-purity CaO production, achieving efficient transformation at 900 °C and 1000 °C with no residual carbonate phases. These results underscore the shells' versatility for use in catalysis, bioceramics, and environmental remediation while supporting waste valorization and circular economy principles [22,23,29].

Physicochemical properties of Hydroxyapatite

The XRD pattern (Fig. 3) of HA derived from *Polymesoda erosa* shells confirms the successful formation of a crystalline HA phase. Prominent diffraction peaks at 2θ angles of 31.7°, 32.9°, and 34.1°, corresponding to the (211), (300), and (202) planes, respectively, match the standard hydroxyapatite (HA) patterns, confirming calcium phosphate as the predominant phase [31,32]. These results align with earlier research on biogenic hydroxyapatite (HA), including HA derived from sand lobster and crab shells, where optimal calcination conditions resulted in distinct and well-defined HA phases. [33,34]. Eggshell-derived hydroxyapatite synthesized via low-power microwave irradiation formed needle-like

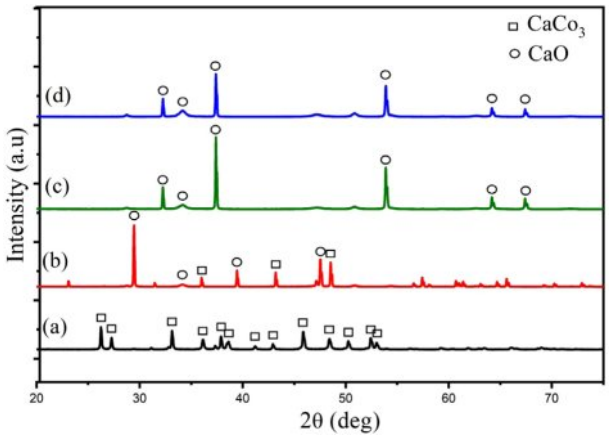

Fig. 1. XRD spectra of *Polymesoda erosa* shell powder: uncalcined, and calcined at 800 °C, 900 °C and 1000 °C.

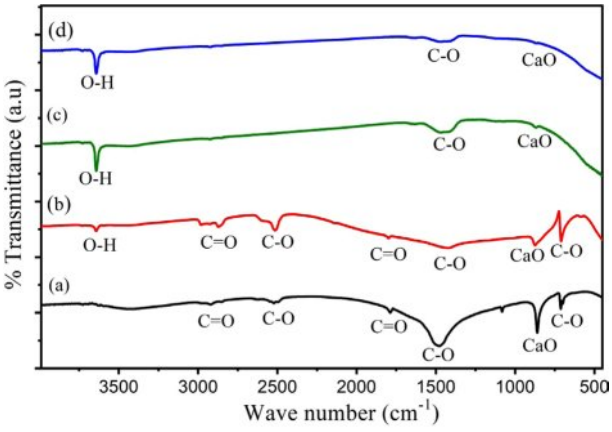

Fig. 2. FTIR spectra of *Polymesoda erosa* shell powder: uncalcined, and calcined at 800 °C, 900 °C and 1000 °C.

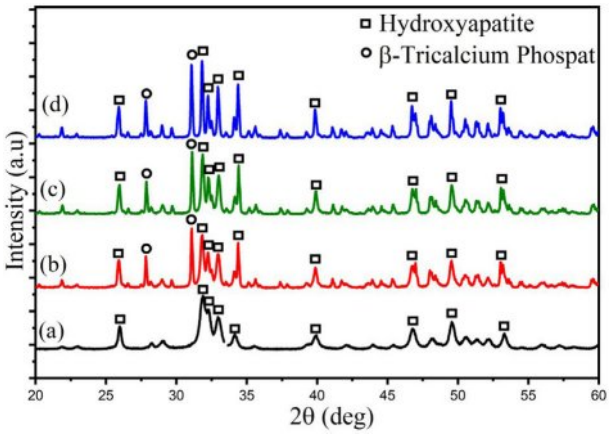

Fig. 3. XRD pattern of HA derived from *Polymesoda erosa* shells.

Table 2. Crystal size, microstrain, lattice parameter, x-ray density and crystallinity of HA.

Sample	Crystallite Size (nm)	Microstrain (ε)	Lattice Parameter (Å)		X-ray Density (g/cm^3)	Crystallinity (%)
			a	c		
HA 700	20.33 ± 1,90	$5.80\times10^{-3} \pm 4.71\times10^{-4}$	9.40	6.87	2.71	65.40
HA 800	32.04 ± 1,91	$3.52\times10^{-3} \pm 2.90\times10^{-4}$	9.40	6.87	2.71	85.50
HA 900	40.43 ± 1,85	$2.80\times10^{-3} \pm 2.79\times10^{-4}$	9.40	6.87	2.71	88.30
HA 1000	48.89 ± 1,60	$1.98\times10^{-3} \pm 1.71\times10^{-4}$	9.40	6.87	2.71	91.10

particles with 22 nm crystallite size for biomedical use [35]. Table 2 highlights the structural properties of the synthesized HA, with crystal sizes in the nanoscale range of 20–50 nm, as calculated using the Scherrer equation. Importantly, at sintering temperatures of 800 °C, 900 °C, and 1000 °C, XRD analysis indicated the development of β-tricalcium phosphate (β-TCP) as a secondary phase. This structural transformation occurred due to the partial decomposition of HA at higher temperatures, a phenomenon commonly observed in biogenic HA sources [33,36]. The presence of β-TCP alongside HA is advantageous for biomedical applications, as β-TCP exhibits enhanced solubility and promotes faster bone regeneration than pure HA [34,37]. As shown in Table 2, the microstrain values indicate moderate lattice strain caused by ionic substitutions and synthesis-induced defects, which enhance bioactivity [38,39]. The lattice parameters and X-ray density remain consistent with other marine- and mineral-derived HA, confirming its suitability for biomedical applications [36,37].

The FTIR spectrum (Fig. 4) corroborates the XRD results by identifying functional groups characteristic of HA. Strong absorption bands at 962 cm^{-1} and 1041 cm^{-1} are attributed to the stretching vibrations of phosphate (PO_4^-) groups, while bands at 568 cm^{-1}, 602 cm^{-1}, and 632 cm^{-1} are linked to the bending vibrations of phosphate (PO_4^-) groups. Additionally, a broad band around 3572 cm^{-1} corresponds to hydroxyl (OH^-) groups. Carbonate (CO_3^-) ions, observed at 1460 cm^{-1}, suggest

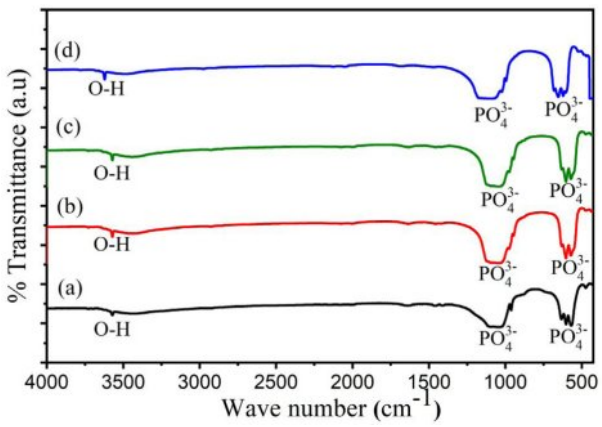

Fig. 4. FTIR pattern of Hydroxyapatite (HA) derived from *Polymesoda erosa* shells.

Table 3. Mineral composition and Ca/P molar ratio of HA.

Element	Mass (%)			
	HA 700	HA 800	HA 900	HA 1000
O	36.79	49.36	50.83	50.87
P	19.85	16.18	16.62	16.42
Ca	43.36	34.45	32.54	32.71
Ca/P molar ratio	1.69	1.65	1.52	1.54

partial substitution of phosphate ions in the HA lattice, enhancing bioactivity and solubility [34,39,40]. These findings are consistent with HA derived from Indonesian limestone, where carbonate retention improves biological integration [36].

The Ca/P molar ratio and mineral composition of HA derived from *Polymesoda erosa* shells, shown in Table 3, further emphasize its similarity to natural bone apatite. At 700 °C, the Ca/P ratio was 1.69, slightly above the stoichiometric value of 1.67, indicating adequate calcium content for bioactivity. At 800 °C, the ratio aligned closely with natural bone at 1.65. However, at 900 °C and 1000 °C, the ratio decreased to 1.52 and 1.54, respectively, due to calcium volatilization and the partial conversion of HA to β-TCP [33,36]. This transformation was advantageous in applications requiring higher solubility and controlled degradation rates, such as bioresorbable implants [34,37]. In previous research, the Ca/P atomic ratios of hydroxyapatite derived from pufferfish teeth were found to be 1.58, 1.64, 1.67, and 1.47 for *Lagocephalus suezensis*, *L. guentheri*, *Sphoeroides pachygaster*, and *Torguigener favimaculasus*, respectively, highlighting their potential for biomedical applications [41].

The SEM and TEM images (Fig. 5) reveal morphological changes in HA with increasing sintering temperatures. At 700 °C, the particles exhibited a fine, porous structure with nanoscale features conducive to bioactivity. At 800 °C and 900 °C, the morphology shifted to a rod-like structure, and β-TCP formation was observed as an additional phase, evidenced by changes in particle size and structure. At 1000 °C, significant grain growth occurred, resulting in larger, crystalline particles. Table 4 shows particle size distributions, which increased with temperature. The average particle size at 700 °C is 78.25 nm (SD = 1.18), which increased to 116.42 nm

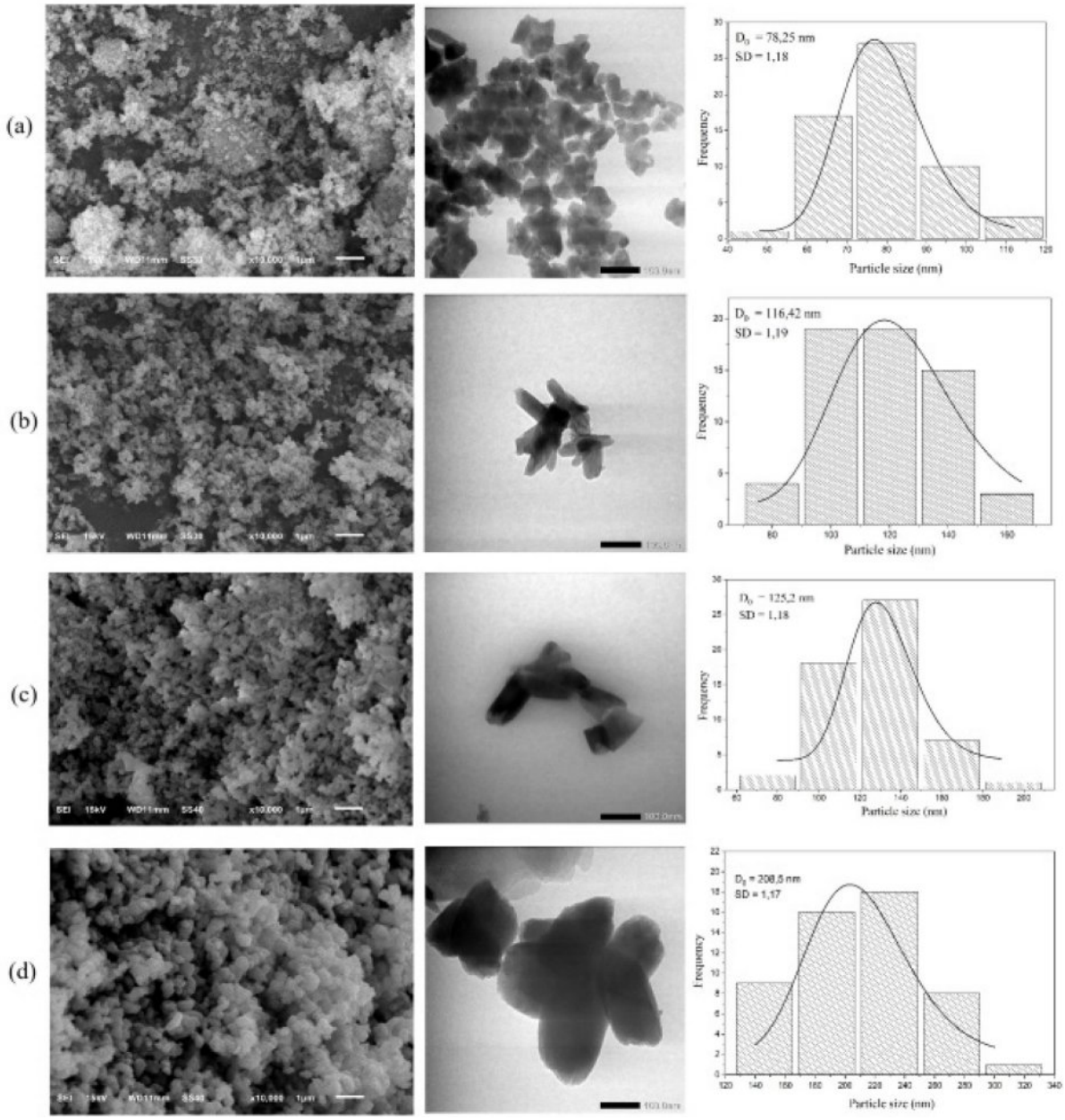

Fig. 5. SEM image, TEM image and particle size distribution patterns of HA at sintering temperatures of (a) 700 ºC, (b) 800 ºC, (c) 900 ºC, and (d) 1000 ºC.

Table 4. The Particle size of HA is derived from *Polymesoda erosa shells.*

Sample	Particle Size (nm)
HA 700	78.25 ± 1.18
HA 800	116.42 ± 1.19
HA 900	125.20 ± 1.18
HA 1000	208.50 ± 1.17

at 800 °C, 125.2 nm at 900 °C, and 208.5 nm at 1000 °C. These trends align with studies on crab shell-derived HA, where increased temperatures similarly induced β-TCP formation and grain growth [34].

Antibacterial activity of Hydroxyapatite-Zinc Oxide (HA-ZnO) composite

HA 700 was selected for HA-ZnO composites, with 700 °C as the optimal doping temperature to achieve the smallest crystal and particle sizes, as well as phase purity, confirmed by XRD and FTIR patterns. At higher sintering temperatures (800-1000 °C), HA transforms into β-TCP. Nanocrystalline structures enhance bioactivity by increasing the surface area-to-volume ratio, improving interaction with biological tissues, and promoting cellular adhesion and proliferation [42,43]. Smaller crystal sizes

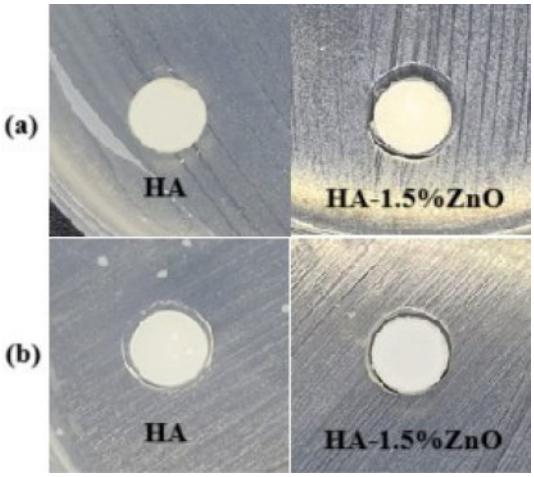

Fig. 6. Zone of Inhibition of HA and HA-1.5% ZnO of (a) *S.Aureus* and (b) *E. coli.*

Table 5. Diameter of Zone of Inhibition.

Bacteria	Diameter (mm)	
	Pure HA	HA-1.5% ZnO
S. Aureus	0	0.96
E. coli	0	0.62

enhance mechanical and biological properties, promoting osteoconductivity and faster bone growth [44,45]. Pure HA is more biocompatible [46].

The antibacterial efficacy of pure HA and the HA-1.5% ZnO composite was evaluated using the zone of inhibition (ZOI) method against *Staphylococcus aureus* (S. aureus) and *Escherichia coli* (E. coli). Pure HA showed no measurable antibacterial activity, whereas the HA-ZnO composite exhibited ZOI diameters of 0.96 mm against *S. aureus* and 0.62 mm against *E. coli*. The larger zone of inhibition against *E. coli* compared to *S. aureus* is due to their structural differences. *E. coli*, a Gram-negative bacterium, has an outer membrane that limits antibacterial agent penetration [47]. In contrast, *S. aureus*, a Gram-positive bacterium, has a thicker peptidoglycan layer, allowing easier penetration of agents [48–50]. The type of antibacterial agent used also influences the results [51].

The findings validate the strong antibacterial properties of ZnO-incorporated biomaterials, in line with prior research. ZnO nanoparticles effectively target both Gram-positive and Gram-negative bacteria through the generation of reactive oxygen species (ROS) and disruption of bacterial membranes, mechanisms that are also observed in the HA-1.5% ZnO composite [52,53]. Compared to pure HA, which showed no antibacterial activity, adding of ZnO improved efficacy. This aligns with previous research, which reported similar zones of inhibition (ZOI) for HA-ZnO composites [53]. The 1.5% ZnO concentration optimizes antibacterial performance while mitigating cytotoxicity concerns associated with higher concentrations. The study results demonstrate that this concentration effectively balances antibacterial efficacy and cytotoxicity, as supported by previous research showing that 1.5% ZnO enhances antibacterial activity without significantly affecting cell viability or mechanical properties [54]. In contrast, concentrations exceeding 5% ZnO lead to increased oxidative stress and apoptosis, reducing cell viability [55]. Additionally, for tissue regeneration applications, lower ZnO concentrations (1-2 wt%) are preferred to promote mesenchymal stem cell survival and differentiation [56]. Uniform ZnO distribution, achieved through precipitation synthesis, further enhances antibacterial performance [57].

Conclusion

This research highlights the viability of using *Polymesoda erosa* shells as an eco-friendly and economical source for producing high-purity HA and HA-ZnO composites, in accordance with circular economy principles. The comprehensive characterization of their structural and antibacterial properties suggests their potential for use in advanced biomedical applications. Calcination of the shells successfully produced high-purity CaO, verified by XRD and FTIR analyses. Partial decomposition of HA into β-TCP was observed at sintering temperatures of 800 °C, 900 °C, and 1000 °C, which improved its solubility and bioactivity, essential for applications in regenerative medicine. The Ca/P molar ratio ranged from 1.52 to 1.69, with values at moderate sintering temperatures resembling natural bone apatite, ensuring compatibility for bone tissue engineering. Incorporating 1.5% ZnO into HA significantly enhanced antibacterial activity, achieving inhibition zones of 0.96 mm against *Staphylococcus aureus* and 0.62 mm against *Escherichia coli*. The optimized ZnO concentration effectively balanced antibacterial performance with cytocompatibility, making HA-ZnO composites suitable for infection-prone applications such as orthopedic and dental implants. These findings confirm the versatility of *Polymesoda erosa* shell-derived HA and HA-ZnO composites as multifunctional biomaterials. Future research should optimize synthesis conditions and explore additional functionalization strategies to expand their applications in diverse medical fields.

Acknowlegnements

The authors would like to express their sincere gratitude to the Indonesian Education Scholarship (BPI), Center for Higher Education Funding and Assessment Ministry of Higher Education, Science, and Technology of Republic Indonesia, Indonesia Endowment Fund for Education (LPDP) for their financial support in conducting this research (00392/J5.2.3./BPI.06/9/2022) and to the Directorate of Research Universitas Gadjah Mada through

the RTA Program for supplemental support (4161/UN1. P1/Dit-Lit/PT.01.01/2025). Additionally, we thank the Laboratory of Material Physics and Instrumentation, Department of Physics and LPPT Universitas Gadjah Mada, for providing the research facilities necessary for this study.

References

1. A. Soulissa and I. Nathania, Sci. Dent. J. 2[1] (2018) 1-9.
2. A.H. Nasution, R.O. Nasution, D.M. Situmorang, and A. Harmaji, J. Appl. Sci. 1[2] (2021) 59-63.
3. J. Kolmas, E. Groszyk, and U. Piotrowska, Nanoscale Res. Lett. 10[278] (2015) 1-9.
4. E. Fiume, G. Magnaterra, A. Rahdar, E. Verné, and F. Baino, Ceramics 4 (2021) 542-583.
5. S.-W. Tsai, Y.-W. Hsu, W. Pan, A. Vadivelmurugan, P. Hwang, and F. Hsu, J. Funct. Biomater. 13[168] (2022) 1-12.
6. M.A. Gani, A.S. Budiatin, M.L.A.D. Lestari, F.A. Rantam, C. Ardianto, and J. Khotib, Materials 15[6] (2022) 1-10.
7. K. Zhang, Y. Zhou, C. Xiao, W. Zhao, H. Wu, J. Tang, Z. Li, S. Yu, X. Li, M. Li, Z. Yu, G. Wang, L. Wang, K. Zhang, X. Yang, X. Zhu, and X. Zhang, Sci. Adv. 5 (2019) 1-16.
8. F.S. Irwansyah, A.R. Noviyanti, D.R. Eddy, and R. Risdiana, Molecules 27[17] (2022) 1-14.
9. C.S. Kumar, K. Dhanaraj, R.M. Vimalathithan, P. Ilaiyaraja, and G. Suresh, J. Asian Ceram. Soc. 8[2] (2020) 416-429.
10. A.F. Abdul Latif, N.A.S.M. Pu'ad, N.A. Akmar Ramli, M.S. Muhamad, H.Z. Abdullah, M.I. Idris, and T.C. Lee, Mater. Sci. Forum 1010 (2020) 584-589.
11. N.A.S.M. Pu'ad, P. Koshy, H.Z. Abdullah, M.I. Idris, and T.C. Lee, Heliyon 5 (2019) 1-14.
12. D.I. Arun, D.A. Mudiyanselage, R.G. Mohamed, M.J. Liddell, N.M. Monsur Hassan, and D. Sharma, Materials 14[1] (2020) 1-15.
13. I. Saleem, N.F. Rana, T. Tanweer, W. Arif, I. Shafique, A.S. Alotaibi, H.A. Almukhlifi, S.A. Alshareef, and F. Menaa, Materials 15[21] (2022) 1-13.
14. P. Huang, S. Xu, W. Liu, C. Liu, H. Ou, Y. Luo, Y. Zhang, X. Zhang, P. Wu, and X. Liao, ACS Appl. Mater. Interfaces 15[5] (2023) 6735-6746.
15. Y. Wang, A. Cao, Y. Jiang, X. Zhang, J. Liu, Y. Liu, and H. Wang, ACS. Appl. Mater. Interfaces 6[4] (2014) 2791-2798.
16. B.A. Sevinç and L. Hanley, J. Biomed. Mater. Res. B Appl. Biomater. 94B[1] (2010) 22-31.
17. J. Liu, J. Shao, Y. Wang, J. Li, H. Liu, A. Wang, A. Hui, and S. Chen, ACS Sustain. Chem. Eng. 7[19] (2019) 16264- 16273.
18. S. Yanova, Jalius, S. Rozi, I. Laksmana, and R. Syelly, IOP Conf. Ser. Earth Environ. Sci., 1st Lekantara Annual Conference on Natural Science and Environment 2021 (IOP Publishing) p.1-5.
19. N.D. Malau, Asian J. Adv. Res. Rep. 18[5] (2024) 164-169.
20. Q. Wang, F. Jiang, X. Ouyang, L. Yang, and Y. Wang, Materials 14[4] (2021) 1-17.
21. B.S. Nugroho, Positron 13[2] (2023) 158-165.
22. D. Summa, M. Lanzoni, G. Castaldelli, E.A. Fano, and E. Tamburini, Resources 11[48] (2022)1-16.
23. S. Seesanong, ACS Omega 8 (2023) 27044-27055.
24. P. George, Life Sci. Med. Biomed. 8[1] (2024) 1-15.
25. M. Yusof, N.T. Razali, N.H.T. Kuan, and D.S. John, J. Appl. Sci. Process Eng. 7[1] (2020) 500-509.
26. Khalil, R.K. Rusli, and. Andri, World Vet. J. 11[4] (2021) 578-586.
27. H. Samouh, S. Nishimoto, H. Yoshida, S. Sawada, O. Kontani, K. Suzuki, and I. Maruyama, J. Adv. Concr. Technol. 19 (2021) 395-413.
28. L. Habte, N. Shiferaw, D. Mulatu, T. Thriveni, C. Ramakrishna, and J.W. Ahn, Sustainability 11[3196] (2019) 1-10.
29. S.W. Sidauruk, D. Iriani, A. Diharmi, A. Anggraini, and A. Azka, IOP Conf. Ser. Earth Environ. Sci. 1118 (2022) 1-7.
30. C.T. Oloyede, S.O. Jekayinfa, A.O. Alade, O. Ogunkunle, O.T. Laseinde, A.O. Adebayo, I. Veza, and I.M.R. Fattah, ChemistrySelect 7 (2022) 1-17.
31. C. Dumitrescu, I.A. Neacșu, V. Surdu, A.I. Nicoara, F. Iordache, R. Trușcă, L.T. Ciocan, A. Ficai, and E. Andronescu, Nanomaterials 11[9] (2021) 2289.
32. A. Almukarramah and Y. Yusuf, Mater. Sci. Forum 975 (2020) 76-81.
33. I.K.H. Dinatha, M.A. Jamilludin, A.I. Supii, H. Wihadmadyatami, J. Partini, and Y. Yusuf, in Mater Sci. Forum (Trans Tech Publications Ltd, 2023), p. 39-44.
34. J. Rohan, D. Thenmuhil, R. Umapriya, and D. Varatharajan, J. Ceram. Process. Res. 23[1] (2022) 22-28.
35. K.W. Goh, Y.H. Wong, R.S.K. Singh, H. Chandran, S.K. Wong, and K.Y.S. Lee, J. Ceram. Process. Res. 23[2] (2022) 158-164.
36. J. Partini, S.M. Bilqis, F.A. Salimy, I. Aziz, M. Sari, N. Cahyati, and Y. Yusuf, J. Ceram. Process. Res. 25[4] (2024) 599-606.
37. M.K. dos Horta, C.B. Westin, D.N. da Rocha, J.B. de Campos, R.F. Magalhães Souza, M.S. Aguilar, and F. Moura, Mater. Res. 26 (2023) 1-8.
38. S.M. Londoño-Restrepo, R. Jeronimo-Cruz, B. Millán-Malo, and E.M. Rivera-Muñoz, Sci. Rep. 9[5915] (2019) 1-12.
39. L.F. Zubieta-Otero, Medcomm – Biomater. Appl. (2023) 1-17.
40. W. Intannia, Sci. Technol Indones. 8 (2023) 486-493.
41. S.A. Doğdu, C. Turan, T. Depci, E. Bahçeci, K. Sangün, and D. Ayas, J. Ceram. Process. Res. 25[1] (2024) 85-91.
42. P. Guo, X. Liu, P. Zhang, Z. He, Z. Li, M. Alini, R.G. Richards, S. Grad, M.J. Stoddart, G. Zhou, X. Zou, D. Chan, W. Tian, D. Chen, M. Gao, Z. Zhou, and S. Liu, Bioact. Mater. 9 (2022) 281-298.
43. J. Chen, G. Zhang, Y. Shen, J. Li, H. Jia, Z. Fang, and Q. Zhang, J. Biomater. Sci. Polym. Ed. 22 (2011) 1-14.
44. S. Bose, S. Dasgupta, S. Tarafder, and A. Bandyopadhyay, Acta. Biomater. 6[9] (2010) 3782-3790.
45. V. Kattimani, S. Kondaka, and K.P. Lingamaneni, Bone Tissue Regener. Insights 7 (2016) 9-19.
46. J. Wu, N. Chen, F. Bai, and Q. Wang, Polym. Compos. (2017) 1-11.
47. A. Usman, S.B. Sanusi, S.M. Lawal, F.M. Musa, and H.M. Auwal, Dutse J. Pure Appl. Sci. 7[4b] (2022) 181-188.
48. M. Fiedot, I. Maliszewska, O. Rac-Rumijowska, P. Suchorska-Woźniak, A. Lewińska, and H. Teterycz, Materials 10[353] (2017) 1-18.
49. O.B. Ahmed and T. Alamro, Sci. Rep. 12 (2022) 1-7.
50. S. Suwanboon, P. Amornpitoksuk, P. Bangrak, A. Sukolrat, and N. Muensit, J. Ceram. Process. Res. 11[5] (2010) 547-551.
51. A. Hui, S. Dong, Y. Kang, Y. Zhou, and A. Wang,

Nanomaterials 9 (2019) 1-13.
52. S. Yuan, Y. Ma, X. Li, Z. Ma, H. Yang, and L. Mu, Materials 13 (2020) 1-10.
53. Charlena, I.H. Suparto, and E. Kurniawan, in IOP Conf. Ser. Mater. Sci. Eng. (IOP Publishing, 2019), pp. 1-7.
54. M. Hussain, S. Arif, Y. Nawab, K. Shaker, and M. Umair, Polym. Compos. 43[2] (2021) 889-905.
55. S. Lü, W. Zhang, R. Zhang, P. Liu, Q. Wang, Y. Shang, M. Wu, K. Donaldson, and Q. Wang, Part. Fibre. Toxicol. 12[5] (2015) 1-12.
56. A. Khader and T.L. Arinzeh, Biotechnol. Bioeng. 117[1] (2019) 194-209.
57. V.R. Sivaperumal, R.J. Mani, V. Polisetti, K. Aruchamy, and T.H. Oh, Molecules 28 (2023) 1-9.